Vibrational Signatures of Protonated, Phosphorylated Amino Acids in the Gas Phase

5 AUTHORS, INCLUDING:

Catarina Correia
King's College London
17 PUBLICATIONS   **342** CITATIONS

SEE PROFILE

Scuderi Debora
Université Paris-Sud 11
72 PUBLICATIONS   **1,015** CITATIONS

SEE PROFILE

Philippe Maître
Université Paris-Sud 11
140 PUBLICATIONS   **3,548** CITATIONS

SEE PROFILE

Gilles Ohanessian
French National Centre for Scientific Resea…
115 PUBLICATIONS   **3,713** CITATIONS

SEE PROFILE

Vibrational Signatures of Protonated, Phosphorylated Amino Acids in the Gas Phase

Catarina F. Correia,[§] Petru O. Balaj,[§] Debora Scuderi,[‡] Philippe Maitre,[‡] and
Gilles Ohanessian*[,§]

*Laboratoire des Mécanismes Réactionnels, Département de Chimie, Ecole Polytechnique, CNRS,
91128 Palaiseau Cedex, France, and the Laboratoire de Chimie Physique, Université Paris-Sud
11, CNRS, 91405 Orsay CEDEX, France*

Received May 29, 2007; E-mail: gilles.ohanessian@polytechnique.fr

Abstract: Structural characterization of protonated phosphorylated serine, threonine, and tyrosine was performed using mid-infrared multiple photon dissociation (IRMPD) spectroscopy and density functional theory (DFT) calculations. The ions were generated and analyzed by an external electrospray source coupled to a Paul ion-trap type mass spectrometer. Their fragmentation was induced by the resonant absorption of multiple photons from a tunable free electron laser (FEL) beam. IRMPD spectra were recorded in the $900-$ 1850 cm^{-1} energy range and compared to the corresponding computed IR spectra. On the basis of the frequency and intensity of two independent bands in the $900-1400$ cm^{-1} energy range, it is possible to identify the phosphorylated residue. IRMPD spectra for a 12-residue fragment of stathmin in its phosphorylated and nonphosphorylated forms were also recorded in the $800-1400$ cm^{-1} energy range. The lack of spectral congestion in the $900-1300$ cm^{-1} region makes their distinction facile. Our results show that IRMPD spectroscopy may became a valuable tool for structural characterization of small phosphorylated peptides.

Introduction

Reversible phosphorylation of the alcohol side chain function of serine (Ser), threonine (Thr), or tyrosine (Tyr) residues is the most frequent post-translational modification (PTM) of proteins. This reversible PTM has very strong impact on protein function. Protein phosphorylation is a ubiquitous mechanism to control various aspects of cell proliferation, differentiation, metabolism, survival, mobility, and gene transcription.[1] Several thousand sites of post-translational phosphorylation are now known, and estimates of the fraction of proteins that are phosphorylated in vivo range as high as 30%.[2] It is often considered that the impact of phosphorylation on protein function is related to the conformational changes it induces. It is therefore of crucial importance to develop techniques to detect, locate, and structurally characterize these modifications in peptides and proteins.

In proteomic studies, tandem mass spectrometry (often abbreviated as "MS/MS") techniques have proven to be powerful tools, with electrospray ionization[3] being the preferred ionization technique. MS/MS provides primary sequence in-

formation for library-based protein identification and the determination of post-translational modifications. Alcohol phosphorylation leads to a mass increase of about 80 Da, depending upon the protonation state of the phosphate. Mass spectrometry is therefore an efficient method to detect the presence of one or more phosphorylations, even for relatively large proteins, provided that high mass accuracy and resolution are available. Collision-induced dissociation (CID) allows the detection of phosphorylated sites based on the loss of characteristic neutrals (-80 Da (HPO_3) and/or -98 Da (H_3PO_4) in positive ion MS/ MS).[4] Infrared multiple photon dissociation (IRMPD) at fixed-wavelength has also been shown to be very effective in the selective fragmentation of phosphorylated vs nonphosphorylated peptides.[5] IRMPD presents one clear advantage over CID: the IR irradiation produced by a CO_2 laser is resonant with one or more phosphate vibrational modes, leading to a much more efficient fragmentation of phosphorylated peptides than for nonphosphorylated ones. This provides an easy way to characterize which peptides are phosphorylated within a complex mixture. This has been achieved in both negative[5] and positive[6] ion modes. Sequencing a peptide should in principle provide the location of any PTM. Upon heating, however, the covalent

§ Ecole Polytechnique.
‡ Université Paris-Sud 11.

(1) Sefton, B. M.; Hunter, T., Eds. *Protein phosphorylation*; Academic Press: New York, 1998.
(2) (a) Blom, N.; Kreegipun, A.; Brunak, S. *Nucleic Acids Res.* **1998**, *26*, 382–386. (b) Kreegipun, A.; Blom, N.; Brunak, S. *Nucleic Acids Res.* **1999**, *27*, 237–239. (c) Diella, F.; Cameron, S.; Gemünd, C.; Linding, R.; Via, A.; Kuster, B.; Sicheritz-Pontén, T.; Blom, N.; Gibson, T. J. *BMC Bioinformatics* **2004**, *5*, 79–83.
(3) Fenn, J. B.; Mann, M.; Meng, C. K.; Wong, S. F.; Whitehouse, C. M. *Science* **1989**, *246*, 64–71.

(4) (a) Huddleston, M. J.; Annan, R. S.; Bean, M. F.; Carr, S. A. *J. Am. Soc. Mass Spectrom.* **1993**, *4*, 710–717. (b) Carr, S. A.; Huddleston, M. J.; Annan, R. S. *Anal. Biochem.* **1996**, *239*, 180–192.
(5) (a) Flora, J. W.; Muddiman, D. C. *Anal. Chem.* **2001**, *73*, 3305–3311. (b) Flora, J. W.; Muddiman, D. C. *J. Am. Chem. Soc.* **2002**, *124*, 6546–6547. (c) Flora, J. W.; Muddiman, *J. Am. Soc. Mass Spectrom.* **2004**, *15*, 121–127.
(6) (a) Crowe, M. C.; Brodbelt, J. S. *J. Am. Soc. Mass Spectrom.* **2004**, *15*, 1581–1592. (b) Crowe, M. C.; Brodbelt, J. S. *Anal. Chem.* **2005**, *77*, 5726–5734.

bonds connecting PTM to peptide or protein backbones are among the most fragile; therefore, they are easily broken upon collisional or IR activation conditions. Recently, the development of electron capture dissociation (ECD) has been prompted in part by the observation that PTMs are preserved under this activation mode.[7] Because ECD sequencing is incomplete, combination of CID and ECD activations is a method of choice for sequencing and PTM localization in phosphopeptides.[8] Until now, however, three-dimensional structural characterization in a mass spectrometric context has remained impossible.

To a large extent, this state of affairs is common to all brands of mass spectrometry. An important breakthrough is now changing this situation, the development of infrared spectroscopy of gas-phase ions within tandem mass spectrometers.[9,10]

Free electron lasers (FEL) have been shown to be particularly suitable for probing the vibrational features of gas-phase ions in the mid-infrared spectral range.[9,10] These FEL provide access to a wide frequency range ($100-2500$ cm^{-1}), and they are sufficiently intense for inducing the IRMPD process for strongly bound ions. The recent developments of optical parametric oscillator/amplifier (OPO/OPA) laser systems make them powerful tools as well to investigate the hydrogen bonds in the near IR range.[11] These spectroscopic tools provide the potential for distinguishing between isomers, and also between conformers, although the latter might be more difficult.[12] This new spectroscopic tool has already found many applications.[12-16] Among them, small biological ions which have been structurally probed by IRMPD include protonated disaccharides,[12a] cationized amino acids,[13] protonated amino esters,[14] protonated and cationized oligopeptides,[12b,14b,15] and a small potassiated protein.[16]

Here we use IRMPD spectroscopy to structurally characterize small models of phosphate-containing biomolecules: protonated, phosphorylated amino acids (pAAH$^+$). These include phosphorylated serine (pSer), threonine (pThr), and tyrosine (pTyr).

While these ions are obviously too simple to provide information relevant to phosphates within "real" biological environments, they do contain some significant structural differences which make them good models to demonstrate the feasibility of this experiment. In particular, pTyrH$^+$ bears a phenyl "spacer" which precludes direct interaction between the protonated amino acid and the phosphate groups, while such interactions are possible in pSerH$^+$ and pThrH$^+$. As will be shown below, IRMPD provides a mean to clearly distinguish between such situations.

In an attempt to assess the potential of IRMPD as a structural probe for phosphate groups in peptides, we have recorded the IRMPD spectra for two peptides bearing a serine residue, one with the serine phosphorylated, YPEFPLpSPPKKK and the other nonphosphorylated, YPEFPLSPPKKK. This 12-residue sequence is a fragment of stathmin, a protein involved in several regulation chains of cell development, depending upon its phosphorylation site(s). Phosphorylation of the serine in the middle of this fragment leads to inhibition of stathmin's activity in microtubule assembly.[17,18]

Experimental Section

1. IRMPD Spectroscopy with the CLIO-FEL. The IRMPD spectra of the pAAH$^+$ were obtained with the CLIO (Centre Laser Infrarouge d'Orsay) IR-FEL coupled to a modified Bruker Esquire 3000+ Paul trap-type mass spectrometer.[19] The IRMPD spectra of the phosphorylated and nonphosphorylated peptides were obtained with the above IR-FEL coupled to a modified Bruker APEX-Qe Fourier Transform Ion Cyclotron Resonance (FT-ICR) mass spectrometer.[20]

The CLIO IR-FEL is based on a 10 to 50 MeV electron linear accelerator.[21] At a given electron energy, the photon energy is tuned by adjusting the undulator gap which is placed in the optical cavity. The IR-FEL output consists of 8 μs long macropulses fired at a repetition rate of 25 Hz. Each macropulse is composed of 500 micropulses, each of a few picoseconds long and separated by 16 ns. For a typical IR average power of 500 mW, the corresponding micropulse and macropulse energies are 40 μJ and 20 mJ, respectively.

The laser wavelength profile was monitored at each reading with a monochromator associated with a pyroelectric detector array (spiricon). The IR-FEL spectral width can be adjusted through a tuning of the optical cavity length, and the laser spectral width (fwhm) was less than 0.5% of the central wavelength.

2. pAA MS Operation Parameters. Phosphorylated amino acids were obtained from Sigma-Aldrich and used without purification. One millimolar pAA solutions were prepared by combining 100 μL of pAA stock solution (10 mM), 1.0 mL of H$_2$O/MeOH 50:50, and and 20 μL of formic acid 98%. Ions were generated by electrospray (ESI), and

(7) Stensballe, A.; Jensen, O.; Olsen, J. V.; Haselmann, K. F.; Zubarev, R. A. *Rapid Commun. Mass Spectrom.* **2000**, *14*, 1793−1800.

(8) (a) Chalmers, M. J.; Håkansson, K.; Johnson, R.; Smith, R.; Shen, J.; Emmett, M. R.; Marshall, A. G. *Proteomics* **2004**, *4*, 970−981. (b) Kocher, T.; Savitski, M. M.; Nielsen, M. L.; Zubarev, R. A. *J. Proteome Res.* **2006**, *5*, 659−668.

(9) (a) Oomens, J.; Van Roij, A. J. A.; Meijer, G.; Von Helden, G. *Astrophys. J.* **2000**, *542*, 404−410. (b) Oomens, J.; Sartakov, B. G.; Meijer, G.; Von Helden, G. *Int. J. Mass Spectrom.* **2006**, *254*, 1−19.

(10) (a) Lemaire, J.; Boissel, P.; Heninger, M.; Mauclaire, G.; Bellec, G.; Mestdagh, H.; Simon, A.; Caer, S. L.; Ortega, J. M.; Glotin, F.; Maitre, P. *Phys. Rev. Lett.* **2002**, *89*, 273002. (b) Maitre, P.; Le Caer, S.; Simon, A.; Jones, W. D.; Lemaire, J.; Mestdagh, H.; Heninger, M.; Mauclaire, G.; Boissel, P.; Prazeres, R.; Glotin, F.; Ortega, J. M. *Nucl. Instrum. Methods Phys. Res. A* **2003**, *507*, 541−546.

(11) See, e.g. Velasquez, J.; Pillai, E. D.; Carnegie, P. D.; Duncan, M. A. *J. Phys. Chem. A* **2006**, *110*, 2325−2330.

(12) (a) Polfer, N. C.; Valle, J. J.; Moore, D. T.; Oomens, J.; Eyler, J. R.; Bendiak, B. *Anal. Chem.* **2006**, *78*, 670−679. (b) Balaj, O. P.; Kapota, C.; Lemaire, J.; Ohanessian, G. *Int. J. Mass Spectrom.* **2008**, *269*, 196−209.

(13) (a) Kapota, C.; Lemaire, J.; Maître, P.; Ohanessian, G. *J. Am. Chem. Soc.* **2004**, *126*, 1836−1842. (b) Polfer, N. C.; Paizs, B.; Snoek, I.; Compagnon, I.; Suhai, S.; von Helden, G.; Meijer, G.; Oomens, J. *J. Am. Chem. Soc.* **2005**, *127*, 8571−8579. (c) Polfer, N. C.; Oomens, J.; Moore, D. T.; von Helden, G.; Meijer, G.; Dunbar, R. C. *J. Am. Chem. Soc.* **2006**, *128*, 517−525. (d) Polfer, N. C.; Oomens, J.; Dunbar, R. C. *Phys. Chem. Chem. Phys.* **2006**, *8*, 2744−2751. (e) Kamariotis, A.; Boyarkin, O. V.; Mercier, S. R.; Beck, R. D.; Bush, M. F.; Williams, E.; Rizzo, T. R. *J. Am. Chem. Soc.* **2006**, *128*, 905−916. (f) Polfer, N. C.; Dunbar, R. C.; Oomens, J. *J. Am. Soc. Mass Spectrom.* **2007**, *18*, 512−516. (g) Bush, M. F.; O'Brien, J. T.; Prell, J. S.; Saykally, R. J.; Williams, E. R. *J. Am. Chem. Soc.* **2007**, *129*, 1612−1622. (h) Bush, M. F.; Forbes, M. W.; Jockusch, R. A.; Oomens, J.; Polfer, N. C.; Saykally, R. J.; Williams, E. R. *J. Phys. Chem A* **2007**, *111*, 7753−7760.

(14) (a) Simon, A.; MacAleese, L.; Maitre, P.; Lemaire, J.; McMahon, T. B. *J. Am. Chem. Soc.* **2007**, *129*, 2829−2840. (b) Wu, R.; MacMahon, T. B. *J. Am. Chem. Soc.* **2007**, *129*, 4864−4865.

(15) (a) Lucas, B.; Gregoire, G.; Lemaire, J.; Maitre, P.; Ortega, J. M.; Rupenyan, A.; Reimann, B.; Schermann, J. P.; Desfrancois, C. *Phys. Chem. Chem. Phys.* **2004**, *6*, 2659−2663. (b) Lucas, B.; Gregoire, G.; Lemaire, J.; Maitre, P.; Glotin, F.; Schermann, J. P.; Desfrancois, C. *Int. J. Mass Spectrom.* **2005**, *243*, 105−113. (c) reference 12b. (d) Marinica, D. C.; Gregoire, G.; Desfrancois, C.; Schermann, J. P.; Borgis, D.; Gaigeot, M. P. *J. Phys. Chem. A* **2006**, *110*, 8802−8810.

(16) Oomens, J.; Polfer, N.; Moore, D. T.; van der Meer, L.; Marshall, A. G.; Eyler, J. R.; Meijer, G.; von Helden, G. *Phys. Chem. Chem. Phys.* **2005**, *7*, 1345−1348.

(17) Marklund, U.; Brattsand, G.; Osterman, O.; Ohlsson, P.-I.; Gullberg, M. *J. Biol. Chem.* **1993**, *268*, 25671−25680.

(18) Redeker, V.; Lachkar, S.; Siavoshian, S.; Charbaut, E.; Rossier, J.; Sobel, A.; Curmi, P. *J. Biol. Chem.* **2000**, *275*, 6841−6849.

(19) (a) Mac Aleese, L.; Simon, A.; McMahon, T. B.; Ortega, J. M.; Scuderi, D.; Lemaire, J.; Maitre, P. *Int. J. Mass Spectrom.* **2006**, *249*, 14−20. (b) Chiavarino, B.; Crestoni, M. E.; Fornarini, S.; Lemaire, J.; Maitre, P.; MacAleese, L. *J. Am. Chem. Soc.* **2006**, *128*, 12553−12561.

(20) Bakker, J. M.; Besson, T.; Lemaire, J.; Scuderi, D.; Maitre, P. *J. Phys. Chem. A* **2007**, *111*, 13415−13423.

(21) Glotin, F.; Ortega, J. M.; Prazeres, R.; Rippon, C. *Nucl. Instrum. Methods Phys. Res. B* **1998**, *144*, 8−17.

the ESI conditions used were as follows: flow rates of 60−80 μL/h and spray voltages of 4700−5000 V with a drying gas temperature of 150 °C.

Details on the performances of the coupling of the CLIO IR-FEL with the modified Bruker Esquire 3000+ Paul trap can be found elsewhere.[19a] The IR-FEL laser beam was focused at the center of the ion trap, by using a 500 mm ZnSe focal lens. A 0.7 mm wide hole drilled in the ring electrode of the trap allows for an optical access to the center of the trap, and the beam position was tuned to maximize the fragmentation efficiency. Multistage mass spectroscopy was carried out using the standard Bruker Esquire Control (version 5.2) software. Within the MS1 step, single isotopes of pAAH$^+$ were mass selected in a 0.5−1 Da mass window. The control of the irradiation time of the ions in the trap was performed using the MS2 step where the excitation amplitude was set to zero. The associated output trigger was used to control the optical shutter, which was then opened for a controlled number of IR-FEL macropulses.

Four different electron energies (40, 42, 45, and 48 MeV) were used in order to optimize the laser power while recording the spectra in the 900−1850 cm^{-1} energy range. The maximum IR power was about 500, 600, 700, and 950 mW for electron energies of 40, 42, 45, and 48 MeV, respectively. While scanning the undulator gap, the power dropped linearly by a factor of 2 at the most. The pSerH$^+$ IRMPD spectrum was recorded using one IR-FEL macropulse (900−1600 cm^{-1}), while the pThrH$^+$ IRMPD spectrum was recorded using one IR-FEL macropulse (900−1000 and 1350−1750 cm^{-1}) and two IR-FEL macropulses (1000−1350 and 1750−1850 cm^{-1}). Finally, the pTyrH$^+$ IRMPD spectrum was recorded using one IR-FEL macropulse (900−1550 cm^{-1}) and three IR-FEL macropulses (1550−1850 cm^{-1}).

3. Peptide MS Operation Parameters. Peptide solutions (55.5 μM) were prepared adding 30 μL of peptide stock solution (1 mM), 0.5 mL of H$_2$O/MeOH 50:50, and 10 μL of formic acid 98%. The ions were generated by electrospray, and the ESI conditions used were as follows: flow rates of 120 μL/h, spray voltages of 4000 V, drying gas flow of 4 L/s, nebulizer pressure of 1.5 bar, and drying gas temperature of 240 °C.

The experiments on the peptides have been performed on a modified FT-ICR mass spectrometer (APEX-Qe Bruker system). The FT-ICR is equipped with an Apollo II ESI ion source, a quadrupole mass filter, a collision cell (hexapole), and a 7 T magnet.

The doubly protonated peptide ions were first mass-selected in the quadrupole mass filter and then accumulated into the collision cell filled with Ar during 500 ms. Subsequently they were accelerated along the axis of the magnetic field, decelerated, and then trapped into the ICR cell at a background pressure of ∼1.5 × 10^{-9} mbar. IRMPD spectroscopy has been performed in the ICR cell by focusing the IR-FEL laser beam with a 2-m focal mirror.[20]

The irradiation time in the ICR cell was adjusted to 400 ms for the phosphorylated peptide and to 1 s for the nonphosphorylated peptide.

4. Theoretical Calculations. The potential energy surfaces of pSerH$^+$, pThrH$^+$, and pTyrH$^+$ were explored at the B3LYP/6-31+G* level. Refined relative energies of all species optimized above were obtained at the B3LYP/6-311++G(2d,2p) level. For the lower energy structures, the IR linear absorption spectra were computed at the B3LYP/6-31+G* level. In a few selected cases, accuracy calibration was carried out via geometry re-optimization and vibrational frequency calculations at the B3LYP/6-311++G(2d,2p) level. All calculations were performed using the Gaussian03 package.[22] The calculated band intensities were convoluted assuming a Lorentzian profile with a 30 cm^{-1} full width at half-maximum (fwhm).

Hybrid DFT methods such as B3LYP have been shown to outperform local or gradient-corrected DFT, as well as MP2, in predicting infrared intensities. An average absolute difference of 20−25 km mol^{-1}

can be expected using B3LYP in conjunction with a large basis set.[23] Calculated frequencies are in general blue-shifted when compared to the experimental ones. These are computed within the harmonic approximation, where anharmonic effects due to coupling of vibrational modes are not taken into consideration. This, together with deficiencies in describing electron correlation within DFT, is expected to contribute to some discrepancies between the experimental and computed frequencies. Provided the use of an appropriate scaling factor, hybrid DFT methods have been shown to be very efficient in reproducing the observed fundamental frequencies, and an average absolute difference of ca. 30 cm^{-1} can be expected using B3LYP.[24] A uniform scaling factor of 0.9614 has been proposed to correct the IR frequencies computed at the B3LYP/6-31G* level.[24,25] This was derived from empirical correlations based on the comparison of experimental and theoretical frequencies for a number of small organic molecules. Several scaling factors specific to phosphorus-containing molecules have also been derived. Among these, corrections were proposed for the P=O and P−O stretching modes.[26] These vary between 0.98 and 1.05. It is worth mentioning that these scaling factors concern specific phosphorus modes of vibration in molecules such as phosphine oxides, phosphines, and phosphorus oxides. Analogous studies for phosphate-containing molecules do not appear to exist to date. As will be discussed below, we have decided to leave our computed frequencies unscaled.

Results and Discussion

Phosphorylated Amino Acids. 1. Experimental Results. The absorption of multiple IR photons by the pAAH$^+$ was probed by monitoring the fragmentation efficiency of the singly charged precursor ion, as a function of photon energy. Let P be the abundance of intact precursor ions and F the sum of the abundances of fragment ion produced by IRMPD at a given photon energy E. IRMPD spectra are obtained by plotting the photofragmentation efficiency, defined as $-\ln(P/F + P)$, as a function of photon energy. For pSerH$^+$ and pThrH$^+$, a loss of 98 Da was observed, corresponding either to the elimination of H$_3$PO$_4$, or of HPO$_3$ and H$_2$O. The fragmentation reaction of pTyrH$^+$ leads to the elimination of 46 Da. On the basis of the fragmentations of TyrH$^+$,[27,28] it is expected that elimination of H$_2$O and CO is involved.

Experimental IRMPD spectra of pSerH$^+$, pThrH$^+$, and pTyrH$^+$ are shown in Figure 1. They were recorded in the 900−1850 cm^{-1} range, with the exception of pSerH$^+$ which was recorded between 900 and 1600 cm^{-1}.

As can be seen, pSerH$^+$ and pThrH$^+$ spectra present several identical features and are distinct from the pTyrH$^+$ spectrum. The latter shows a single strong absorption band in the 900−1150 cm^{-1} region against two intense bands for pSerH$^+$ and pThrH$^+$. On the other hand, pSerH$^+$ and pThrH$^+$ present one broad band at 1150−1400 cm^{-1}, against three well spaced distinct bands in the same region for pTyrH$^+$. As already shown in previous experiments,[19a] the fwhm of IRMPD bands in the Paul ion trap is about 20−25 cm^{-1}. This suggests that the broad band observed at 1150 cm^{-1} for pSerH$^+$ and pThrH$^+$ is probably

(22) Frisch, M. J.; et al. Gaussian03 Rev. B.05, Pittsburgh, PA, Gaussian, Inc., 2003.

(23) Halls, M. D.; Schlegel, H. B. *J. Chem. Phys.* **1998**, *109*, 10587−10593.
(24) Wong, M. W. *Chem. Phys. Lett.* **1996**, *256*, 391−399.
(25) Irikura, K. K.; Johnson, R. D.; Kacker, R. N. *J. Phys. Chem. A* **2005**, *109*, 8430−8437.
(26) (a) Katsyuba, S.; Vandyukova, E. *Chem. Phys. Lett.* **2003**, *377*, 658−662. (b) Jensen, J. O.; Banerjee, A.; Zeroka, D.; Merrow, C. N.; Gilliam, S. J.; Kirkby, S. J. *Spectrochim. Acta Part A* **2004**, *60*, 1947−1955.
(27) (a) El Aribi, H. E.; Orlova, G.; Hopkinson, A. C.; Siu, K. W. M. *J. Phys. Chem. A* **2004**, *108*, 3844−3853. (b) Zhao, J.; Shoeib, T.; Siu, K. W. M.; Hopkinson, A. C. *Int. J. Mass Spectrom.* **2006**, *256*, 265−278.
(28) Rogalewicz, F.; Hoppilliard, Y.; Ohanessian, G. *Int. J. Mass Spectrom.* **2000**, *196*, 565−590.
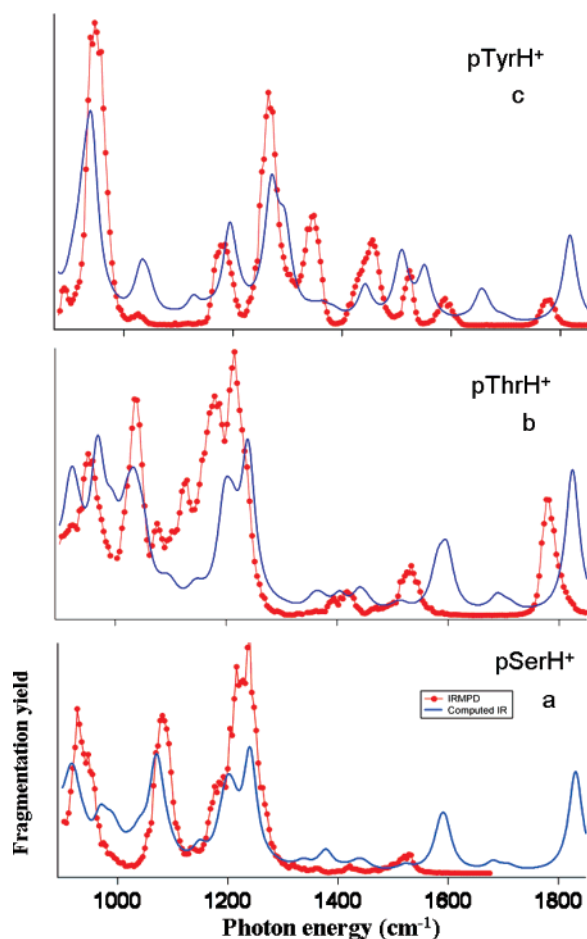
Figure 1. Experimental IRMPD and simulated IR absorption spectra of the lowest energy pAAH$^+$ rotamers, computed at the B3LYP/6-31+G* level. Each simulated spectrum was obtained by weighting the IR intensities of the computed spectrum for each rotamer by its Maxwell−Boltzmann population and by convoluting the results by a Lorentzian profile with a fwhm of 30 cm^{-1}. Experimental spectra are fragmentation efficiencies defined as $-\ln(P/F + P)$, with F being the sum of fragment abundances and P the abundance of the intact precursor.

due to several partially unresolved bands. In the 1400−1600 cm^{-1} energy range pSerH$^+$, pThrH$^+$, and pTyrH$^+$ show one, two, and three small signals, respectively. Finally, the pThrH$^+$ and pTyrH$^+$ spectra display one single band at 1750−1800 cm^{-1}.

2. Assignment of the Experimental IR Absorption Spectra of pAAH$^+$. The identification of the vibrational signatures of phosphorylation is accomplished by the assignment of experimental IRMPD bands for each pAAH$^+$, using the computed IR vibrational bands of the corresponding more stable structures. Therefore, the first step is to identify these structures. The pAAH$^+$ are likely to show several isomers. These arise from the protonation of one of the following groups: amine, carboxylic acid, phosphate, oxygen from phosphate ester, and aromatic ring (for pTyrH$^+$). At room-temperature each isomer may exist as a mixture of several rotamers, which arise from rotations around the P−OH bonds in the phosphate group.

Table 1 present the Gibbs free energies of calculated pAAH$^+$ structures. For each pAAH$^+$, the most stable isomer corresponds to the protonation of the amine group as expected, considering its high proton affinity. The pSerH$^+$ and pThrH$^+$ structures show a hydrogen bond between the protonated amine and the P=O bond of the phosphate. Such interaction is absent in pTyrH$^+$

Table 1. Relative Gibbs Free Energies of pAAH$^+$ Isomers at 298 K

isomers	ΔG,[a] kJ mol^{-1}		
	pSerH$^+$	pThrH$^+$	pTyrH$^+$
NH$_3^+$	0	0	0
phosphate H$^+$	51	52	74
(COOH)H$^+$	53	48	92
aromatic ring H$^+$	-	-	105
ester phosphate H$^+$	206	182	197

[a] Computed at the B3LYP/6-311++(2d,2p)//B3LYP/6-31+G* level. The most stable rotamer is considered for each isomer.

because of the aromatic "spacer" ring that lies in between. As mentioned above, this feature is expected to influence the vibrational signature of the P=O bond. The ammonium charge in pTyrH$^+$ is stabilized by N−H⋯π bonding in all low-energy rotamers. This is similar to what has recently been described for TyrH$^+$.[29]

The magnitude of the free energy differences (>50 kJ mol^{-1}) between the amine protonated structures and the other isomers should rule out their coexistence before irradiation. The geometries and computed IR spectra for pSerH$^+$ isomers, along with the corresponding experimental IRMPD bands, are displayed in Figure 2. While there is a good match between the experimental bands near 950 and 1100 cm^{-1} and the bands computed for the phosphate-protonated isomer, it is not the case for the main band between 1200 and 1250 cm^{-1}. As can be seen, the best agreement between computation and experiment is observed for the amine protonated isomer, which is the lowest energy structure. The same conclusion holds true for pThrH$^+$ and pTyrH$^+$.

Under our experimental conditions, multiple collisions between pAAH$^+$ ions and helium buffer gas provide an efficient thermalization of the ions. Assuming that the ions are at room temperature, each amine-protonated isomer should present several rotamers. The relative energies of each rotamer protonated in the amine group are presented in Table 2. Their geometries are presented in Figures 3 and 4, with exception of pThrH$^+$ rotamers presented as Supporting Information. Being close in energy (<10 kJ mol^{-1}), these rotamers are likely to significantly contribute to the experimental IRMPD spectra, broadening the IRMPD band shapes. Even though the accuracy of energy differences between rotamers is not expected to be better than ± 3 kJ mol^{-1}, the values in Table 2 show that a significant mixing certainly occurs. Figure 5 shows the difference between pSerH$^+$ theoretical spectra of the most stable rotamer and of the Maxwell−Boltzmann weighted mixture of conformers at 298 K. As can be seen, these contributions should be taken into account in the computed spectra used for the assignment of the experimental results. Instead of simply comparing the experimental bands for each pAAH$^+$ with the computed spectra of their corresponding most stable rotamers, we have used the Maxwell−Boltzmann distribution to estimate the fraction of population associated to each rotamer at 298 K (see Table 2). Finally, the convolution of the above results by a Lorentzian profile with a full width at half-maximum (fwhm) of 30 cm^{-1} led to the theoretical spectra presented in Figure 1.

(29) Stearns, J. A.; Mercier, S.; Seaiby, C.; Guidi, M.; Boyarkin, O. V.; Rizzo, T. R. *J. Am. Chem. Soc.* **2006**, *129*, 11814−11820.
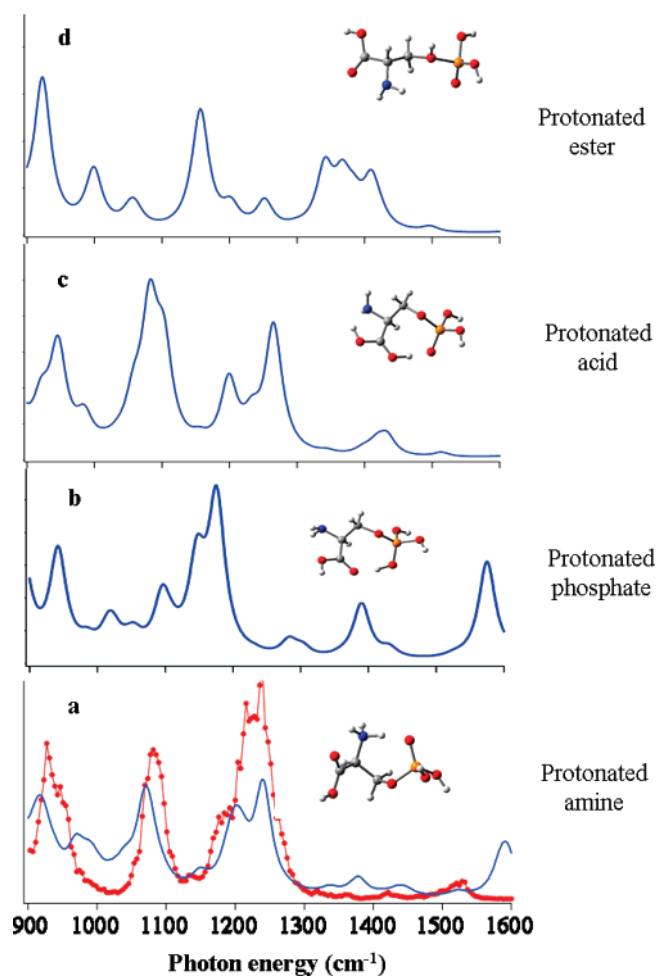
Figure 2. Comparison between the experimental IRMPD spectrum of pSerH⁺ (a) and the theoretical convoluted IR spectra of the lowest energy pSerH⁺ isomers (a–d), computed at the B3LYP/6-31+G* level. Structures of the lowest energy isomers of pSerH⁺ correspond to the protonation of the amine (a), phosphate (b), carboxylic acid (c), and oxygen from the phosphate ester groups (d), respectively.

Table 2. Relative Gibbs Free Energies and Maxwell−Boltzmann Populations at 298 K for the Amine-Protonated pAAH⁺ Rotamers

	pSerH⁺		pThrH⁺		pTyrH⁺	
rotamer	ΔG^a	$\%^b$	ΔG^a	$\%^b$	ΔG^a	$\%^b$
1a	0	40	0	38	0	53.7
1b	1.2	24	0.5	32	0.4	33.7
1c	1.5	22	2.1	17	11	0.4
1d	2.5	14	2.3	16	-	-

a Computed at the B3LYP/6-311++(2d,2p)//B3LYP/6-31+G* level. Values in kJ mol⁻¹. *b* According to the Maxwell−Boltzmann distribution at 298 K.

3. Assignment of the Experimental IR Absorption Spectra of Protonated Phosphoserine and Phosphothreonine. The computed IR bands and corresponding modes for the most stable rotamers of pSerH⁺ and pThrH⁺ are described in Tables 3 and 4, respectively. The experimental IRMPD bands are shown in Figure 1 and reported in Tables 3 and 4 for pSerH⁺ and pThrH⁺, respectively. As can be seen in Figure 1, the main features are very similar in both cases. The first broad band (920−970 cm⁻¹ range for pSerH⁺, around 960 cm⁻¹ for pThrH⁺) can be assigned to the coupling of P−OH stretching and POH bending modes of the phosphate group with the backbone C−C stretching and
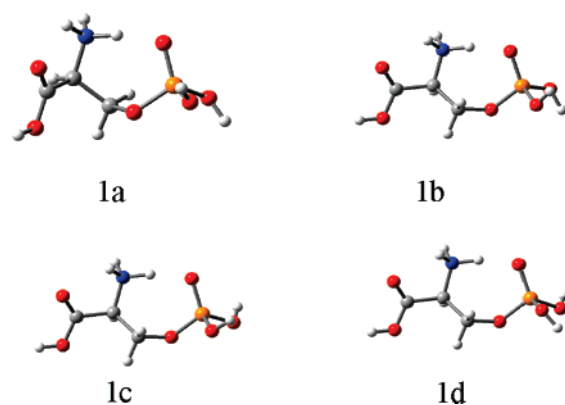

Figure 3. Optimized geometries of amine protonated pSerH⁺ most stable rotamers.
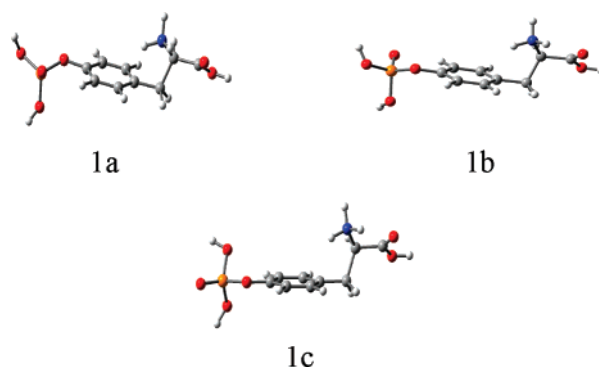

Figure 4. Optimized geometries of amine protonated pTyrH⁺ most stable rotamers.
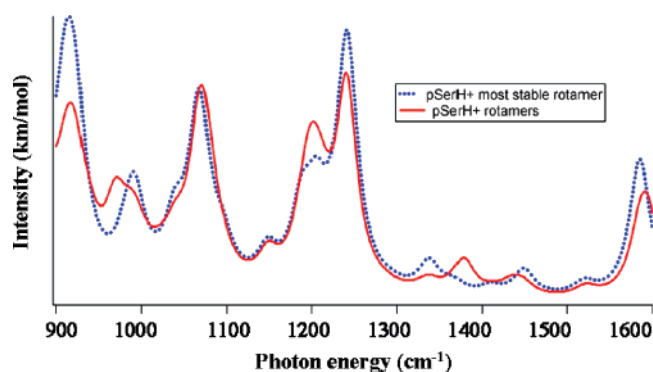

Figure 5. Comparison of pSerH⁺ theoretical spectrum for the most stable rotamer (1a) with the convoluted spectrum of rotamers **1a−d** computed at the B3LYP/6-31+G* level.

NH₃⁺ rocking. The second broad band (around 1080 and 1040 cm⁻¹ for pSerH⁺ and pThrH⁺, respectively) is due to the coupling of P−OH stretching and POH bending modes, with the PO−C and C−OH stretches. An additional band at 1130 cm⁻¹ for pThrH⁺ is due to its methyl group. The third and most intense experimental band apparently results from the partial overlap of two unresolved bands for pSerH⁺, which are slightly more splitted for pThrH⁺. The first (less intense, around 1190 or 1180 cm⁻¹) is assigned to the coupling of C−OH stretching and COH bending modes from the carboxylic acid, with NH₃⁺ rocking (plus CH₃ rocking for pThrH⁺). The other one (more intense, around 1230 or 1220 cm⁻¹) is assigned to the P=O stretch. The last common experimental band, located around

Table 3. Measured (left Column) and Calculated Vibrational Frequencies for pSerH$^+$ More Stable Rotamers. The Reported Calculated IR Intensities (km/mol, in Parentheses) for Each Rotamer Result from Multiplication of Computed Intensities by the Corresponding Maxwell−Boltzmann Factor

IRMPD	wavenumber (cm^{-1})				vibrational mode
	1a	1b	1c	1d	
927	914 (24)	915 (33)	922 (111)	923 (211)	ν C−C, ν P−OH, δ POH, δ_r NH$_3^+$
947	969 (253)	939 (110)			δ POH, ν P−OH
1081	1075 (185)	1075 (79)	1069 (174)	1068 (254)	ν P−OH, δ POH, ν PO−C, ν C−OH
1192	1195 (124)	1198 (74)	1198 (107)	1188 (97)	ν C−OH, δ COH, δ_r NH$_3^+$
1228		1211 (390)			ν P=O, δ POH
	1241 (199)		1241 (202)	1242 (350)	
	1379 (48)	1379 (30)	1379 (43)	1338 (43)	δ COH, δ CCH
1529	1596 (104)		1594 (86)	1585 (194)	δ_{umb} NH$_3^+$
a	1681 (20)	1681 (13)	1681 (21)	1711 (24)	δ_{sciss} NH$_3^+$
a	1831 (167)	1831 (103)	1832 (150)	1831 (266)	ν C=O, δ COH

^{a} This part of the IRMPD spectrum was not recorded.

Table 4. Measured (left Column) and Calculated Vibrational Frequencies for pThrH$^+$ More Stable Rotamers. The Reported Intensities (km/mol, in Parentheses) for Each Rotamer Result from Multiplication of Computed Intensities by the Corresponding Maxwell−Boltzmann Factor

IRMPD	wavenumber (cm^{-1})				vibrational mode
	1a	1b	1c	1d	
935		917 (29)	927 (209)	914 (113)	ν C−C, δ POH, δ COH, δ_r NH$_3^+$,
967	967 (138)	938 (69)	968 (163)	921 (46)	ν P−OH, δ POH
	1019 (15)		1022 (196)	995 (149)	δ POH, ν P−OH, ν N−H
1035	1034 (132)	1051 (77)	1034 (72)	1036 (71)	ν P−OH, δ POH, ν PO−C, ν N−H
1076	1068 (254)	1069 (269)	1075 (109)	1075 (86)	ν PO−C, ν C−C, δ_r CH$_3$
1130	1143 (37)	1140 (7)	1141 (5)	1140 (3)	δ_r CH$_3$, δ_r NH$_3^+$
1179	1198 (86)	1198 (80)	1198 (166)	1195 (97)	δ_r CH$_3$, ν C−OH
1216		1212 (151)		1211 (91)	ν P=O, δ POH
	1241 (132)		1238 (296)	1241 (333)	
1394	1404 (17)		1406 (29)	1405 (16)	δ COH, δ C−H
1418	1440 (18)	1439 (18)	1439 (35)	1446 (20)	δ COH, ν C−OH, δ_r NH$_3^+$, δ_{umb} CH$_3$
1534	1596 (72)	1598 (66)	1598 (134)	1581 (196)	δ_{umb} NH$_3^+$
1777	1831 (113)	1824 (108)	1825 (224)	1825 (277)	ν C=O, δ COH

Table 5. Measured (left Column) and Calculated Vibrational Frequencies for pTyrH$^+$ More Stable Rotamers. The Reported Intensities (km/mol, in Parentheses) for Each Rotamer Result from Multiplication of Computed Intensities by the Corresponding Maxwell−Boltzmann Factor

IRMPD	wavenumber (cm^{-1})			vibrational mode
	1a	1b	1c	
946	926 (530)	925 (445)	936 (25)	ν P−OH, δ POH, ν C=C,^{a} ν PO−C,
1026	1032 (64)	1034 (50)	1030 (6)	δ POH, δ CCH^a
	1046 (69)	1045 (63)	1050 (127)	δ POH
1185	1194 (292)	1194 (223)	1194 (28)	ν C−OH, δ COH
1265	1271 (365)	1271 (341)	1281 (50)	ν PO−C, ν C=C,^{a} δ CCH^a
	1294 (156)	1296 (198)		δ POH, ν P=O
1348	1442 (106)	1443 (90)	1442 (11)	δ COH, δ CCH, δ_r NH$_3^+$
1456	1511 (120)	1511 (132)	1512 (15)	δ_{umb} NH$_3^+$
1523	1552 (159)	1552 (135)	1553 (15)	δ CCH,^{a} ν C=C^a
1589	1665 (34)	1663 (27)	1664 (3)	$\delta_{scissor}$ NH$_3^+$
1781	1818 (282)	1817 (238)	1818 (30)	ν C=O, δ COH

^{a} Denotes aromatic ring.

1530 cm^{-1}, can be assigned to the NH$_3^+$ umbrella mode. Finally, the C=O stretch of the carboxylic acid group arises near 1780 cm^{-1} for pThrH$^+$ (not measured for pSerH$^+$).

4. Assignment of the Experimental IR Absorption Spectrum of Protonated Phosphotyrosine. The computed IR bands and corresponding modes for pTyrH$^+$ most stable rotamers are listed in Table 5. The experimental IRMPD spectrum is shown in Figure 1, and the positions of the IRMPD bands are reported in Table 5. The first and most intense IRMPD band at 946 cm^{-1} is assigned to the coupling of P−OH stretching and POH bending modes of phosphate group with C=C aromatic stretches and with the PO−C stretch. The region of 1100−1400 cm^{-1} displays three well spaced bands. The first (around 1185 cm^{-1}) may be attributed to C−OH stretching and COH bending modes. The second (around 1270 cm^{-1}) is assigned to the P=O stretching mode, coupled with PO−C and C=C aromatic stretches and POH and CCH aromatic bends. The third one (around 1350 cm^{-1}) is due to COH and CCH bendings, coupled with NH$_3^+$ rocking. The next band in the spectrum, located around 1460 cm^{-1}, is assigned to the umbrella mode of NH$_3^+$, while the following one arises from the coupling of aromatic CCH bends with C=C stretches. The small band around 1590 cm^{-1} is probably arising from the coupling of the above-described modes with NH$_3^+$ scissoring. Finally, the last band
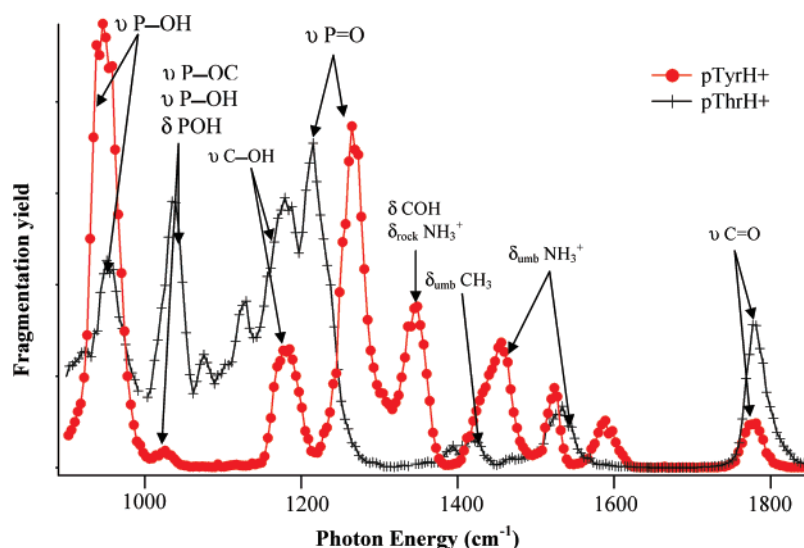
Figure 6. Superposition of experimental IRMPD spectra of pThrH$^+$ and pTyrH$^+$ with corresponding band assignment.

in the spectrum, located at 1780 cm^{-1}, is attributed to the C=O stretch.

5. Discussion. Overall, the convoluted theoretical IR bands are in good agreement with the observed experimental IRMPD bands (Figure 1). Before discussing each experimental spectrum in details, there are some general features that need to be considered. Because of the multiple photon absorption process associated to the IRMPD process, comparison of the resulting IRMPD spectra with computed IR absorption spectra is a priori difficult. On the basis of experiments on a large variety of systems, it seems, however, that IRMPD and linear infrared absorption spectra tend to be very close.[9b] This validates the procedure of using computed frequencies to assign the experimental IRMPD bands. The experimental bands are well resolved. Their width is probably due the result of the combination of multiphoton effects, laser bandwidth, temperature of the ions, and coexistence of several rotamers during irradiation. The intensities of the observed IRMPD bands are not very well reproduced in the theoretical spectra. However, it is known that accurate theoretical prediction of vibrational intensities requires medium to large size basis sets with an adequate number of polarization and diffuse functions, more complete than the 6-31+G* basis set used to compute the IR frequencies. As a result, IR frequencies tend to be better predicted than IR intensities by quantum chemical calculations.[23,24]

As mentioned above, hybrid DFT methods can accurately predict IR frequencies, provided the use of an appropriate scaling factor. In the present case, we chose not to scale the calculated frequencies, and we would like to justify this choice. As can be seen in Figure 1, the computed bands in the 900−1300 cm^{-1} region reproduce the position of the corresponding experimental bands reasonably well, and a uniform scaling of calculated frequencies would not adequately correct the theoretical bands. On the other hand, the use of specific scaling factors for each mode of vibration would be difficult since some of the phosphate bands result from strong coupling with non-phosphate vibrations. It thus seems that there is no straightforward procedure to correct the theoretical spectra for anharmonic effects. In the absence of reliable scaling factors for molecules bearing a phosphate group, we have decided to leave our computed frequencies unscaled. This explains some of the observed discrepancies

between experimental and computed bands, especially for those concerning non-phosphate modes of vibration, in the region of 1400−1800 cm^{-1}. These are systematically blue-shifted when compared with their corresponding experimental bands. Within this region, the use of the standard scaling factor for B3LYP/6-31+G* (0.9614)[24,25] would significantly improve the agreement between the theoretical and experimental frequencies.

As mentioned above, our aim was to find and identify the vibrational signatures of the phosphate group. The phosphate vibrational signatures appear in the 900−1300 cm^{-1} energy range for all pAAH$^+$ (Tables 3−5). As mentioned above, the pSerH$^+$ and pThrH$^+$ spectra are very similar in this spectral range. In order to support the following discussion, experimental IRMPD spectra of pThrH$^+$ and pTyrH$^+$ are compared in Figure 6.

Despite the differences in the relative IR intensity of the bands, both theoretical spectra display two bands in the 900−1000 cm^{-1} region (Figure 1). These are apparently not well resolved in the experimental spectra. An analogous band is also present in the IRMPD spectrum of pTyrH$^+$ and is well reproduced by a single band in the theoretical spectrum. The second broad band, also present in all experimental spectra appears to be more useful for structural characterization of phosphorylated peptides. This one is also assigned essentially to phosphate modes of vibration such as P−OH stretch and POH bend, together with PO−C stretch. In pSerH$^+$ and pThrH$^+$ it appears as an intense sharp band around 1080 and 1035 cm^{-1}, respectively. Being 50 cm^{-1} apart, both are well reproduced in the corresponding computed spectra. On the contrary, in the case of pTyrH$^+$, this same band appears as a very weak signal in the IRMPD spectrum.

The most striking signature of the environment of the phosphate group can be derived from the analysis of the difference between the pAAH$^+$ experimental spectra within the 1150−1400 cm^{-1} region (Figures 1 and 6). In the cases of pSerH$^+$ and pThrH$^+$, the main feature observed below 1250 cm^{-1} corresponds to two overlapping bands (Figure 1), in good agreement with the simulated spectra. On the other hand, the pTyrH$^+$ experimental spectrum displays three well resolved bands at 1185, 1265, and 1348 cm^{-1}. The less intense feature observed at ∼1180−1190 for all three pAAH$^+$ corresponds to

non-phosphate modes of vibration. The most intense contribution, however, is essentially due to the P=O stretch mode: it is observed at 1265 cm^{-1} for pTyrH$^+$ and at lower frequencies (1228 and 1216 cm^{-1}) for pSerH$^+$ and pThrH$^+$. This band constitutes an important vibrational signature of phosphorylation, and its position is dependent upon the surrounding environment. Indeed, as mentioned above, the big structural difference between these molecules relies on the aromatic ring present in pTyrH$^+$ side chain. This rigid spacer disables the direct interaction between the P=O bond and the protonated amine group. On the contrary, pSerH$^+$ and pThrH$^+$ side chains are small and flexible enough to allow for direct hydrogen bonding interaction between P=O and [H−NH$_2$]$^+$ groups. The direct consequence of this intramolecular hydrogen bond is the red-shift of the stretch frequency of hydrogen-bonded P=O by 40−50 cm^{-1} (Figure 6). It thus seems that it should be experimentally possible to distinguish a phosphorylated tyrosine from a phosphorylated serine or threonine, based only on the stretching frequency of the P=O bond of the phosphate group. Possible difficulties in extending this conclusion to phosphorylated peptides are discussed below.

The 1400−1800 cm^{-1} energy range is free of phosphate signatures. Nonetheless, as can be seen in Figure 6, the IRMPD band assigned to the NH$_3^+$ umbrella mode is observed at different frequencies depending on the nature of the amino acid. This band is observed at a higher frequency for pSerH$^+$ and pThrH$^+$ (∼1530 cm^{-1}) than for pTyrH$^+$ (∼1460 cm^{-1}). This effect is clearly related to the above-discussed structural difference between pSerH$^+$ and pThrH$^+$ on one hand, and pTyrH$^+$ on the other. In the former case, there is a strong hydrogen bond, with an N−H···O=P distance of about 1.6 Å, while in the latter there is no direct interaction between the P=O and the protonated amine. A much weaker hydrogen bond exists between the protonated amine and the carbonyl oxygen of the carboxylic acid in pTyrH$^+$. The net result of having the ammonium group involved in a hydrogen bond is an impediment of the umbrella motion as observed for protonated amino acids.[14a,19a] It is therefore not surprising that this mode is found blue-shifted for pSerH$^+$ and pThrH$^+$, as compared to pTyrH$^+$.

The C=O stretching band of the carboxylic acid group is found at nearly the same frequency for pThrH$^+$ and pTyrH$^+$ (Figure 6). This further confirms that the hydrogen bond between the ammonium group and the CO carboxylic group is weak. The pSerH$^+$ experimental spectrum was only recorded below 1600 cm^{-1}, and it is expected to be similar to that of pThrH$^+$ in the higher wave number region. The NH$_3^+$ umbrella and C=O stretching bands are well reproduced in all computed spectra. The pTyrH$^+$ spectrum presents one additional small band related to the NH$_3^+$ scissoring mode. Its presence is predicted in both pThrH$^+$ and pTyrH$^+$ computed spectra (see Table 4 and 5, respectively), but it is only observed for pTyrH$^+$. It should be noticed that the 1600−1780 cm^{-1} range was explored under different experimental conditions. Since the IR-FEL laser power slowly decreases when increasing the photon energy, this part of the spectrum was also recorded using an electron energy of 48 MeV. Despite these more favorable conditions, no IRMPD band of pThrH$^+$ was found in the 1600−1780 cm^{-1} range, probably due to the relatively weak IR absorption cross-section. Finally, the pThrH$^+$ experimental spectrum presents two weak signals around 1400 cm^{-1}, that are absent in the pSerH$^+$

spectrum. The more intense peak is related to the CH$_3$ umbrella mode of vibration and is evidence of the difference between these two residues (the methyl group in pThrH$^+$ side chain).

Phosphorylated and Nonphosphorylated Peptides. 1. Experimental Results. IRMPD spectra of two peptides in their doubly protonated forms have been recorded in the 800−1400 cm^{-1} spectral energy range. These peptides correspond to a 12-residue fragment of stathmin in its phosphorylated and non-phosphorylated forms. Upon IR activation, multiple fragments can be observed as illustrated in the mass spectra displayed in Figure 7. It is expected that infrared irradiation generates fragment ions similar to those observable under collisional activation.

As can be seen in Figure 7, fragmentation of the phosphorylated peptide leads to the elimination of H$_3$PO$_4$, or of HPO$_3$ and H$_2$O, yielding several doubly charged ions (e.g., [M − H$_3$PO$_4$]$^{2+}$ at m/z 706.9, [y$_9$−H$_3$PO$_4$]$^+$ at m/z 1023.7, and [b$_7$−H$_3$PO$_4$]$^+$ at m/z 816.4). Additionally, fragmentation leads to C-terminal product ions (e.g., y$_9^+$ at m/z 1121.7, y$_8^+$ at m/z 975.5). The fragmentation of the nonphosphorylated peptide leads to N-terminal product ions (e.g., b$_{11}^{2+}$ at m/z 642.9, b$_{11}^+$ at m/z 1284.7, and b$_{10}^+$ at m/z 1156.6), as well as internal product ions, that have dissociated at both termini (e.g., b$_{11}$y$_{10}^{2+}$ at m/z 512.3, b$_{11}$y$_{10}^+$ at m/z 1023.7, and b$_{10}$y$_{10}^+$ at m/z 895.6).

The IRMPD spectra for the two doubly protonated peptides were recorded in the 800−1400 cm^{-1} range, as displayed in Figure 8. It can be seen that essentially no fragmentation is observed between 800 and 1000 cm^{-1}. Intense features are observed in both spectra at higher photon energies. For the nonphosphorylated peptide, a single band is observed in the 1060−1180 cm^{-1} region, with a maximum near 1140 cm^{-1}. It is large enough that it may be the result of several unresolved bands. Indeed, on the basis of previous experiments performed using the same experimental setup, IRMPD bandwidth (fwhm) of ∼20 cm^{-1} has been characterized when the IR-FEL laser is on resonance with an isolated IR absorption band of mass-selected ions.[20] The IRMPD spectrum of the phosphorylated peptide strongly differs from the nonphosphorylated case, with significant absorption from 1000 to 1350 cm^{-1}.

2. Discussion. The above discussion for the phosphorylated amino acids suggests that phosphate vibrational signatures can be used to identify the site of phosphorylation and structurally characterize the surrounding environment. The question at hand is whether these conclusions still hold true for more complex systems.

As can be seen in Figure 8, no fragmentation is observed between 800 and 1000 cm^{-1}. Intense features are observed in both spectra at higher photon energies. For the non phosphorylated case, a single asymmetric band is observed in the 1060−1180 cm^{-1} region, with a maximum near 1140 cm^{-1}. It is large enough that it may be the overlapping of several unresolved bands. The IRMPD spectrum of the phosphorylated peptide is completely different. An IRMPD signal is observed from 1000 to 1350 cm^{-1}, and at least two structured bands can be distinguished. Since photofragment intensity does not drop anywhere near the baseline between these two bands, it may be hypothesized that the modes which are infrared-active in the nonphosphorylated peptide are present here as well. A shoulder near 1320 cm^{-1} may also correspond to an additional vibrational band of lower intensity. Inspection of these two IRMPD spectra
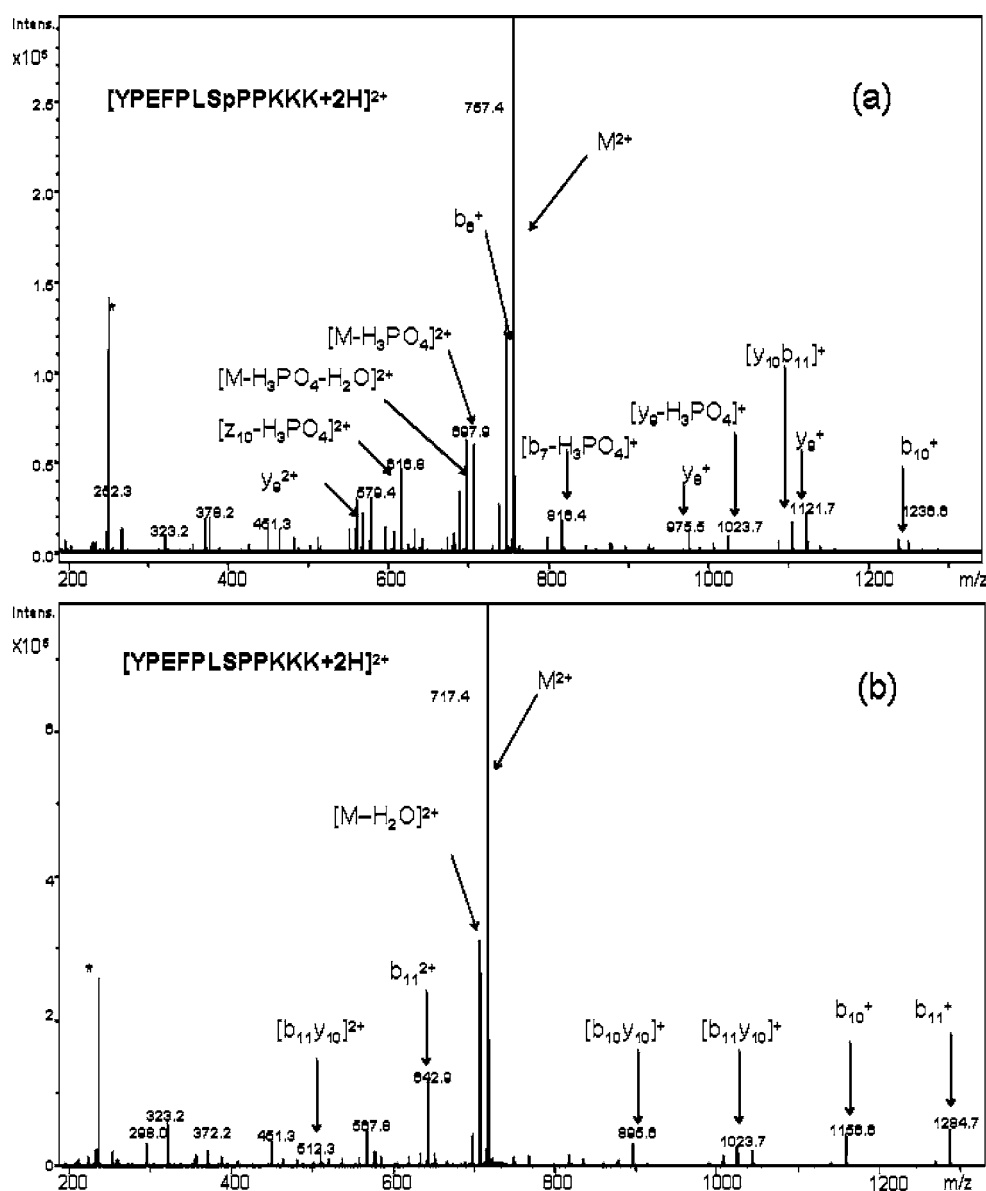
Figure 7. FT-ICR IRMPD MS/MS spectra of the phosphorylated (a) and nonphosphorylated (b) doubly protonated peptides. Peaks due to electronic noise are labeled with an asterisk.
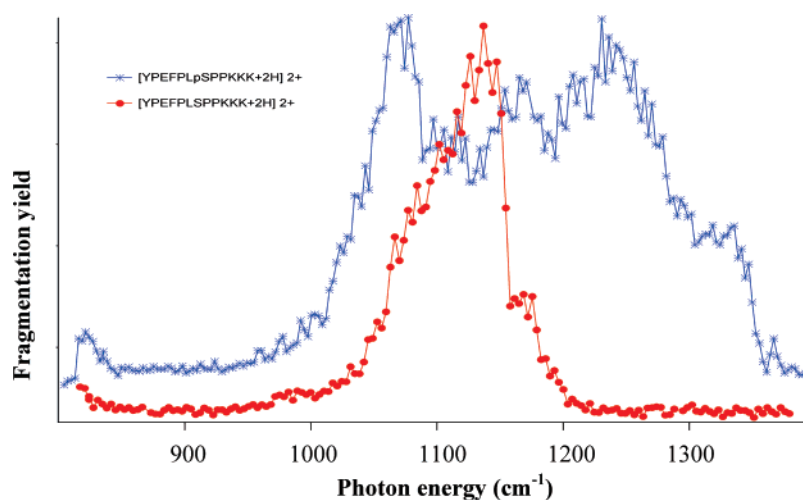

Figure 8. Experimental IRMPD spectra of the doubly protonated peptides. Fragmentation yields are as defined in the legend of Figure 1.

shows that phosphorylation induces a dramatic change in the $1000-1300$ cm^{-1} wavenumber range.

Even though this change could in principle be attributed to an overall conformational transition of the peptide upon phosphorylation, comparison of the IRMPD spectrum of [YPEFPLpSPPKKK+2H]$^{2+}$ with those of the three protonated, phosphorylated amino acids indicates that the new bands are probably due to the phosphate group. Inspection of the positions of the IRMPD bands for the three pAAH$^+$ may suggest that the phosphorylated peptide band around 1080 cm^{-1} is the signature of the pSerH$^+$ group. Indeed, an IRMPD band is observed at 1081 cm^{-1} for pSerH$^+$, while the corresponding band appears at 1035 cm^{-1} for pThrH$^+$ and is very weak for pTyrH$^+$. Assuming that the position of this band is not strongly shifted by the peptide environment (see below), it may be considered diagnostic of the presence of a phosphorylated serine. Similarly, the band of the phosphorylated peptide around 1240 cm^{-1} could be the signature of the P=O stretch. The corresponding IRMPD band was observed at 1128 and 1216 cm^{-1}, for pSerH$^+$ and pThrH$^+$, and at a higher frequency, 1265 cm^{-1}, for pTyrH$^+$ where P=O is not involved in a H-bond with the ammonium group. Although this assignment of the main two bands of [YPEFPLpSPPKKK + 2H]$^{2+}$ at 1070 and 1240 cm^{-1} to phosphate-based modes seems highly reasonable, it was deemed important to obtain further insight into how they may be influenced by the phosphate environment in the peptide.

On the basis of their sequences, the peptides studied here have four basic sites, the three lysine (K) side chains on the C-terminal side, and the N-terminal amine of the main chain. One may then assume that the two protons carrying the charges are distributed among these four sites, although charge solvation may also stabilize protonation at other locations. In fact, it is likely that charge solvation between two lysine side chains is the most favorable. On the basis of these assumptions, there should be at least one lysine protonated. Given the proximity of the three lysines to the phosphorylated serine in the sequence, it is likely that an H-bond can be established between the P=O and at least one amine side chain, although it is not possible to decide whether it is protonated or not without further structural information. In order to obtain indications on the possible influence of such interactions on the phosphate vibrational properties, we have resorted to quantum chemical modeling. Since all of the four most basic sites are primary amines, the model used is a phosphoserine interacting with a methylamine, either neutral or protonated.

Structures optimized at the B3LYP/6-31+G* for the noncovalent complexes pSer-CH$_3$NH$_2$ and pSer-CH$_3$NH$_3^+$ are shown in Figure 9. Relative energies in kJ mol^{-1} obtained at the B3LYP/6-311+G(2d,2p) level are also given (in parentheses) but will not be discussed since the purpose of studying these model complexes is essentially to derive the IR signatures associated with the various possible orientations of hydrogen bonds to and from the phosphate group.

For pSer-CH$_3$NH$_2$, structure **1** involves chelation by the methylamine as a H-bond donor to the P=O of the phosphate and to the amine nitrogen. In structure **2**, methylamine chelates the phosphate, as an H-bond acceptor from one PO—H and as a donor to the P=O. In structure **3**, methylamine chelates both phosphate POH groups, one the PO—H being an H-bond donor, the other an H-bond acceptor. For pSer-CH$_3$NH$_3^+$, structures **1**
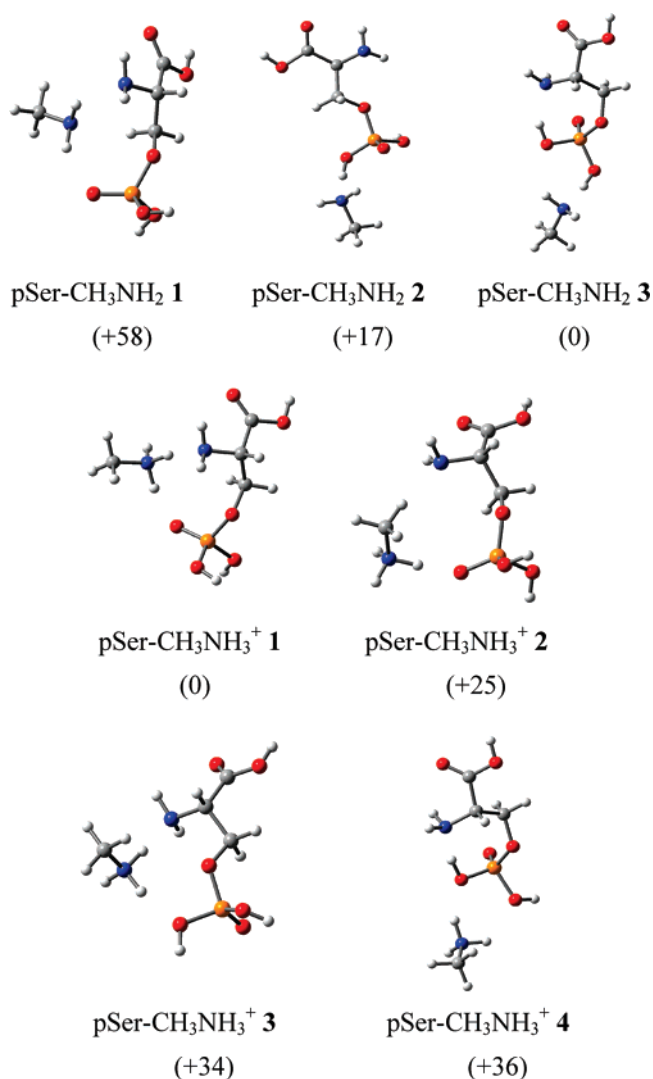

Figure 9. Structures for pSer-CH$_3$NH$_2$ and pSer-CH$_3$NH$_3^+$ noncovalent complexes, optimized at the B3LYP/6-31+G* level. Relative energies in kJ mol^{-1} (obtained at the B3LYP/6-311+G(2d,2p) level) are given in parentheses.

pSer-CH$_3$NH$_2$ **1** (+58)
pSer-CH$_3$NH$_2$ **2** (+17)
pSer-CH$_3$NH$_2$ **3** (0)

pSer-CH$_3$NH$_3^+$ **1** (0)
pSer-CH$_3$NH$_3^+$ **2** (+25)

pSer-CH$_3$NH$_3^+$ **3** (+34)
pSer-CH$_3$NH$_3^+$ **4** (+36)

and **3** are very similar to those of pSer-CH$_3$NH$_2$, while in structure **2** the methylamonium interacts with the P=O bond only, and in structure **4** it is a H-bond donor to one of the HO—P oxygens and to the amine nitrogen.

As discussed above, the experimental IRMPD band centered at 1240 cm^{-1} corresponds very well to a mode with a main P=O stretch component, which lies at 1228 cm^{-1} in pSerH$^+$. In structures **1** and **2** of pSer-CH$_3$NH$_3^+$, in which there is H-bond interaction between the ammonium and the P=O bond, this band is at 1258 and 1241 cm^{-1}, respectively. In structures **3** and **4**, in which the P=O bond has no strong interaction with any other group, this band is at 1308 and 1301 cm^{-1}, respectively. This suggests that the presence of a positive charge in the vicinity of the P=O bond induces a red-shift of its stretching frequency by about 60 cm^{-1}. Finally, we should note that the presence of a charge, with its strong polarizing effect, has more influence than that of an H-bond. This is illustrated by the comparison of the calculated IR absorption spectra of structures 1 and 2 of pSer-CH$_3$NH$_2$: in structure **1**, the P=O stretch frequency is 1306 cm^{-1}, while it is 1263 cm^{-1} in structure **2**.

The COH bending mode in the most stable structure of pSerH$^+$ is at 1197 cm^{-1}, which is a typical value for a free acid. The lack of significant absorption near 1200 cm^{-1} in the nonphosphorylated peptide indicates that the C-terminal acid is probably involved in a H-bond. For the phosphorylated peptide, however, the strong absorption in this region precludes a similar conclusion. The P—OH stretching and POH bending modes of the phosphate are also highly sensitive to hydrogen bonding and to the presence of a charge, in terms of both frequency and intensity, as is expected for highly polar bonds. Moreover, as discussed previously, these two POH modes are often strongly coupled to backbone modes of the entire residue. This makes it more difficult to suggest an assignment of the absorptions observed in the phosphorylated peptide, on the basis of our modeling. Nevertheless, the broad band with a maximum near 1070–1080 cm^{-1} agrees very well with the band at 1090 cm^{-1} in pSerH$^+$. In the methylamine complexes, computations indicate again that coupling of the P—OH stretching and POH bending modes, sometimes also strongly coupled to the P—OC stretch, lead to intense bands between 1000 and 1100 cm^{-1}, depending upon the isomer considered. However at this stage, there is no clear explanation for the absence of other POH-related bands between 900 and 1000 cm^{-1}.

In the previous discussion, we have assumed that the two positive charges of the peptides correspond to the only sites bearing a net charge. One may also consider the possibility of a salt-bridge, in which a deprotonated phosphate would interact with one or two positive charges (protonated groups) out of a total of three. In a 12-residue peptide, coexistence of three positive charges may imply strong repulsion. This scenario is much more difficult to model and has not been considered in the present work.

The question of the nature of the band at 1050–1150 cm^{-1} in the spectrum of the nonphosphorylated peptide may also be discussed on the basis of previous work[14b] on related systems. IRMPD spectra and quantum chemical calculations on Tyr-K$^+$ and Phe-K$^+$ indicate that the aromatic side chains have vibrational bands below 1100 cm^{-1} (Phe) and above (Tyr), which can be assigned to combinations of C—C stretching and CH bending deformations, plus the COH bending for Tyr. The COH bending mode of the carboxylic acid is also found in the 1140–1170 cm^{-1} range when it is involved in a hydrogen bond. The IRMPD spectrum of YGGFL-K$^+$ [14b] bears a feature in a wavenumber range very similar to the one observed in Figure 8. The presence of one Tyr and one Phe residue in the peptide considered here makes it reasonable that this band arises from modes of the aromatic side chains. These are of course also present in the phosphorylated peptide, leading to a very broad absorption.

The results obtained in the previous sections indicate that phosphate groups have intense and specific vibrational bands in gaseous ions. In addition, some of these bands may be sensitive enough to the phosphate environment that they may be considered as potential structural probes. One condition for this to be useful is that the phosphate bands arise in a relatively "silent" region of the vibrational spectra of peptides and proteins; otherwise, they might be buried in an intense signal which would be difficult to resolve. This is not clear yet, as the use of IRMPD for large biomolecules remains very limited. The only previous IRMPD study of a gaseous macromolecular ion to date,

cyctochrome c (a 104-residue protein),[16] was restricted to the 1420–1780 cm^{-1} wavenumber range, i.e., out of the region of interest for phosphate probing. There has also been a study of two potassiated peptides, RPPGF-K$^+$ and YGGFL-K$^+$,[13b] whose IRMPD spectra have been recorded in the 800–1800 cm^{-1} range. These spectra display no significant feature in the 800–1100 cm^{-1} region; however, there are bands with significant intensity between 1100 and 1200 cm^{-1}. In the 1200–1300 cm^{-1} range, absorption appears to be limited. On the basis of these results, and because of the limited resolution inherent to spectroscopy at room temperature, it remains to be demonstrated that specific peaks may be identified without ambiguity in this region.

Conclusions

IRMPD spectroscopy has proven to be a valuable tool for identifying the vibrational signatures of phosphorylated amino acid residues. Because of the strong polarity of the P=O and P—O bonds, phosphate groups have intense IRMPD bands. These strongly IR active vibrational modes can be observed in the 900–1300 cm^{-1} wavenumber range, a region which is partly IR-silent for peptides, in between the functional group absorption in the fingerprint region, and the delocalized backbone modes below 1000 cm^{-1}. This favorable situation leads to characteristic phosphate bands, which are expected to remain identifiable in phosphorylated peptides. On the basis of the position and intensity of two independent bands in the 900–1400 cm^{-1} energy range, it is possible to identify the phosphorylated residue. These are respectively associated to the P=O stretch, and to P—O—H stretching and bending modes of vibration. The P=O stretching band is very sensitive to its surrounding environment. In the case of pSerH$^+$ and pThrH$^+$, characterized by a strong H-bond between the ammonium and the P=O group, the P=O stretching frequency is near 1220 cm^{-1}. In the case of pTyrH$^+$, where the P=O group can be considered as free, the P=O frequency is observed at 1265 cm^{-1}. On the other hand the band associated to P—OH stretching and bending modes is a valuable signature since it appears as a very weak signal in the pTyrH$^+$ IRMPD spectrum and as an intense sharp band separated by 50 cm^{-1} for pSerH$^+$ and pThrH$^+$.

The present results indicate that some of the phosphate bands allow for distinguishing which residue is phosphorylated and for deciphering some of the features of its immediate environment. Moreover, the spectra recorded for a 12-residue peptide in both its phosphorylated and nonphosphorylated forms demonstrate that the lack of spectral congestion in the 900–1300 cm^{-1} region makes their distinction easy. The overall conclusion is that these phosphate vibrational signatures may become valuable tools in the structural characterization of phosphorylated sites, provided that spectral congestion remains limited for larger peptides. Work is underway to extend these studies to other phosphorylated peptides and to proteins.

Coupling IR CO$_2$ lasers to mass spectrometers is now routine and commercially available. Coupling FEL lasers to ion traps is now turning IRMPD from another dissociation technique to a full spectroscopic tool. While such setups are too complex to be disseminated, the recent development of benchtop OPO/OPA lasers opens the promise of commercial availability of tunable IRMPD within the coming years. This may add great value to the mass spectrometric approaches developed on MS platforms.

Supporting Information Available: Complete reference 22 and Figure 10 showing the optimized geometries of amine protonated pThrH$^+$ most stable rotamers. This material is available free of charge via the Internet at http://pubs.acs.org.

JA073868Z